Acta Cryst. (1992). B48, 764–769

Structural Parameters and Electron Difference Density in $BaTiO_3$

BY R. H. BUTTNER AND E. N. MASLEN

Physics Department, University of Western Australia, Nedlands, Western Australia 6009, *Australia*

(*Received* 21 *January* 1992; *accepted* 5 *May* 1992)

Abstract

Barium titanate, $BaTiO_3$, $M_r = 233.24$, tetragonal, $P4mm$, $a = 3.9998$ (8), $c = 4.0180$ (8) Å, $V = 64.281$ (3) Å^3, $Z = 1$, $D_x = 6.024$ Mg m^{-3}, λ(Mo $K\alpha$) = 0.71069 Å, $\mu = 18.60$ mm^{-1}, $F(000) = 102$, $T = 298$ K, $R = 0.013$, $wR = 0.013$ for 243 unique reflections. Structural parameters and electron difference densities for $BaTiO_3$ determined from two sets of X-ray diffraction data measured independently with Mo $K\alpha$ radiation are in close agreement. The average cubic structure, the average centrosymmetric tetragonal structure and the correct non-centrosymmetric structure were refined, and the difference density $\Delta\rho$ was evaluated for each model. In the non-centrosymmetric model the z and U_{33} parameters are highly correlated, but the least-squares refinements were stable. The O-atom vibrations along the Ti—O bonds are smaller than the Ti amplitudes. The atomic charges reflect the combined effects of electronegativities and the electron depletion due to the close packing of the Ba atoms in the structure. In the centrosymmetric average structures the topography of $\Delta\rho$ resembles that observed for cubic $SrTiO_3$. For the correct non-centrosymmetric structure the topography of $\Delta\rho$ near the Ti nucleus has the characteristics required for stability at that position.

Introduction

The ferroelectric properties of $BaTiO_3$ were discovered by von Hippel, Breckenridge, Chesley & Tisza (1946). The tetragonal room-temperature phase, originally assigned to the space group $P4/mmm$ (Megaw, 1945, 1946, 1947) was shown to conform to the non-centrosymmetric space group $P4mm$ by convergent-beam electron diffraction (Tanaka & Lempfuhl, 1972), definitely confirming indications by other techniques (Rhodes, 1949; Frazer, Danner & Pepinsky, 1955; Danner, Frazer & Pepinsky, 1960; Evans, 1951, 1961; Harada, Pedersen & Barnea, 1970). This $P4mm$ structure is stable from 268 to 393 K. $BaTiO_3$ undergoes phase transitions to orthorhombic at 268 K and to rhombohedral at 183 K. Above 393 K the stable phase has the ideal cubic structure with space group $Pm\bar{3}m$. The tetragonal, orthorhombic and rhombohedral phases are polar and ferroelectric (Evans, 1961). There is an additional hexagonal modification reported by Megaw (1946) and by Burbank & Evans (1948).

The changes in the structural parameters from the ideal cubic phase to the room-temperature phase, which are small, may be considered in two stages. The first, which reduces the symmetry from $Pm\bar{3}m$ to $P4/mmm$, involves slight contraction of the a and b axes, and extension of the c axis. Three equivalent O atoms in the cubic structure become O1, at the centre of the ab face, with two symmetry-related O2 atoms at the centres of the ac and bc faces. In the second stage of the symmetry reduction, the Ti, O1 and O2 atoms are displaced by unequal distances parallel to the c axis, forming the non-centrosymmetric $P4mm$ structure. Although deviations from the ideal atomic radii facilitate this reorganization, atom size is unlikely to be the driving force because that would involve antisymmetric displacements of O1 atoms arising from an essentially symmetric crystal field.

The magnitudes of the X-ray structure factors reflect the changes in the structural parameters only to second order (Buerger, 1960), and are thus rather small. The changes of the structure-factor phases in the non-centrosymmetric structure are first order in the structural distortion, but reflection phases are not accessed directly in diffraction experiments. Because of the second-order dependence of structure-factor magnitudes on this structural distortion the least-squares refinement is unusually sensitive to the accuracy of the intensity measurements. The stability of the refinement is an indicator of the quality of the measured structure factors.

The electron density has been evaluated for a wide range of perovskite structures, including other alkaline-earth titanates (Buttner, 1990). The consistency of the residual electron density in $BaTiO_3$ with those for the related perovskites provides a further test of the accuracy of the measured structure factors.

Experimental

Crystals were prepared by the flux-growth method used by Sugi, Hasegawa & Ohara (1968) to crystal-

0108-7681/92/060764-06$06.00

Table 1. *Experimental and refinement data for* $BaTiO_3$

	Model (1)[a]		Model (2)[b]		Model (3)[c]	
	Data set (1)	Data set (2)	Data set (1)	Data set (2)	Data set (1)	Data set (2)
R_{int} (before absorption)	0.032	0.039	0.027	0.031	0.027	0.031
R_{int} (after absorption)	0.031	0.034	0.025	0.031	0.025	0.031
No. of independent reflections	99	99	243	243	243	243
hkl range	$0\le h\le 4, 0\le k\le 6, 0\le l\le 8$		$0\le h\le 6, 0\le k\le 8, 0\le l\le 8$		$0\le h\le 6, 0\le k\le 8, 0\le l\le 8$	
No. of refined parameters	6	6	11	11	14	14
R	0.012	0.010	0.013	0.012	0.013	0.013
wR	0.013	0.010	0.013	0.013	0.013	0.013
S	4.0 (3)	2.9 (2)	3.7 (2)	3.2 (2)	3.7 (2)	3.2 (2)
Min. $\Delta\rho$ (e Å^{-3})	−3.1 (1)	−1.9 (1)	−3.9 (1)	−3.5 (1)	−3.8 (1)	−3.7 (1)
Max. $\Delta\rho$ (e Å^{-3})	0.8 (1)	1.1 (1)	0.9 (1)	1.2 (1)	1.1 (1)	1.3 (1)

Notes: (*a*) Cubic, $Pm\bar{3}m$. (*b*) Centrosymmetric, tetragonal, *P4/mmm*. (*c*) Non-centrosymmetric, tetragonal, *P4mm*.

lize $SrTiO_3$. A mixture of $KF:KMoO_4:BaTiO_3$ in the molar ratio 60:30:10 was heated to 1323 K and cooled by approximately 15 K h^{-1}. Some of the $BaTiO_3$ crystals obtained were tetragonal prisms. The translucent appearance of colourless regular hexagons was consistent with their having undergone a phase transition. Distorted amber hexagonal crystals with $a = b = 5.719$ (1), $c = 13.958$ (8) Å were of the form analysed by Burbank & Evans (1948).

After eliminating any crystals that were strongly affected by extinction, cell dimensions, peak profiles and equivalent reflection intensities for several tetragonal prisms were checked. The best results were obtained from a specimen with (±100), (0±10) and (00±1) faces 30.7, 25.0 and 25.5 μm respectively from a common origin within the crystal. Two data sets were measured on a Syntex $P2_1$ diffractometer, using graphite-monochromatized Mo $K\alpha$ radiation with mean wavelength $\lambda = 0.71069$ Å. Unit-cell dimensions from six reflections $41.43 \le 2\theta \le 41.64°$ (for both sets) $a = 3.9998$ (8), $c = 4.0180$ (8) Å. Scan type $\omega/2\theta$. Scan speed 4.88° min^{-1}. Background measurement one third of total scan time. Scan width $(a + b\tan\theta)$ 1.7 and 0.7°. $2\theta_{max} = 100°$. $-8 \le h \le 8$, $-8 \le k \le 8$, $-8 \le l \le 8$. $(\sin\theta/\lambda)_{max} = 1.08$ Å^{-1}. Number of reflections measured 3604 and 3464 for data sets (1) and (2) respectively. Standards ±400, ±030, ±004 measured every 100 reflections with maximum variation 1.2 and 1.1% for sets (1) and (2) respectively. Analytical absorption correction (Alcock, 1974), Lorentz and polarization corrections applied. Transmission range 0.39, 0.47 and 0.40, 0.47 for (1) and (2). Variances in measured structure factors $\sigma^2(F_o)$ from counting statistics, modified for source instability using the program *DIFDAT* and increased when necessary by applying the Fisher test option of program *SORTRF* (Hall & Stewart, 1989) when comparing intensities of equivalent reflections. Full-matrix least-squares refinement, weights $w = 1/\sigma^2(F_o)$ for all independent reflections, *i.e.* following good statistical practice, no reflections were classified arbitrarily as 'unobserved'. Experimental and refinement details are given in Table 1.† Atomic scattering factors of Cromer & Mann (1968) with the anomalous-dispersion corrections of Cromer & Liberman (1970). Relativistic scattering factors from *International Tables for X-ray Crystallography* (1974, Vol. IV), were applied in a refinement to check the validity of the use of those of Cromer & Mann (1968). The differences were not significant. Lorentz, polarization and absorption factors evaluated analytically. Least-squares residual $\sum w|F_o - F_c|^2$ minimized by adjusting the scale, and variable position and vibration parameters, along with r^* for the Zachariasen (1969) isotropic secondary-extinction corrections as formulated by Larson (1970). Minimum extinction factor $y = 0.93$ for both data sets. Final shift/e.s.d. < 0.0001. Computer programs *STARTX*, *DIFDAT*, *ABSORB*, *ADDATM*, *ADDREF*, *FC*, *CRYLSQ*, *BONDLA*, *FOURR*, *CHARGE*, *CONTRS*, *SLANT* and *PLOT* from the *XTAL*2.6 system (Hall & Stewart, 1989), installed on a SUN 280 computer, were used.

Structure models

Model structures were refined assuming (1) the average cubic cell with $Pm\bar{3}m$ symmetry, (2) the centrosymmetrically averaged *P4/mmm* tetragonal structure and (3) the correct non-centrosymmetric *P4mm* structure. The equivalent cubic cell dimension was set at 4.006 (2) Å. Friedel pairs were averaged and merged even in case (3) because the effects of anomalous dispersion are very small (Buerger, 1960). Parameters for the refinements are listed in Table 2.

For models (1) and (2) the differences between the structural parameters for the two data sets are consistent within the standard deviations. The large off-diagonal element values between z and U_{33}

† Lists of structure factors and the correlation matrix for the non-centrosymmetric refinement of data set (1) have been deposited with the British Library Document Supply Centre as Supplementary Publication No. SUP 55254 (4 pp.). Copies may be obtained through The Technical Editor, International Union of Crystallography, 5 Abbey Square, Chester CH1 2HU, England. [CIF reference: AS0598]

Table 2. *Atomic coordinates and anisotropic thermal parameters, U* ($Å^2 \times 10^5$)

Data set (2) follows the data set (1) result for each column entry. $T = \exp[-2\pi^2(a^{*2}h^2U_{11} + b^{*2}k^2U_{22} + c^{*2}l^2U_{33})]$. $U_{12} = U_{13} = U_{23} = 0$.

	x	y	$z^{a,b}$	z^c	$U_{11} = U_{22}{}^a$	$U_{11}{}^b$	$U_{11}{}^c$	$U_{22}{}^b$	$U_{22}{}^c$	$U_{33}{}^a$	$U_{33}{}^b$	$U_{33}{}^c$
Ba	0.0	0.0	0.0	0.0	541 (9)	525 (6)	523 (6)	525 (6)	523 (6)	541 (9)	594 (10)	666 (21)
					547 (7)	533 (6)	530 (7)	533 (6)	530 (7)	547 (7)	579 (8)	592 (33)
Ti	0.5	0.5	0.5	0.482 (1)	880 (17)	837 (14)	834 (14)	837 (14)	834 (14)	880 (17)	965 (31)	266 (117)
				0.490 (10)	889 (13)	859 (13)	853 (19)	859 (13)	853 (19)	889 (13)	931 (30)	688 (437)
O1	0.5	0.5	0.0	0.016 (5)	704 (47)	695 (51)	721 (51)	695 (51)	721 (51)	724 (74)	916 (116)	729 (162)
				0.019 (13)	703 (37)	686 (47)	715 (67)	686 (47)	715 (67)	737 (58)	868 (96)	556 (704)
O2	0.5	0.0	0.5	0.515 (3)	704 (47)	680 (56)	700 (57)	649 (56)	669 (57)	724 (74)	785 (53)	647 (101)
				0.517 (10)	703 (37)	626 (50)	649 (70)	691 (51)	713 (70)	737 (58)	809 (70)	583 (434)

Notes: (*a*) Model (1). (*b*) Model (2). (*c*) Model (3) (see Table 1 for definitions).

Table 3. *Interaction vector lengths* (Å) *from data set* (1) *for* $BaTiO_3$

	Ba—Ti	Ti—Ti	Ba—O1	Ba—O2	Ti—O1	Ti—O2
Model (1)	3.4691 (8)	4.0058 (8)	2.8325 (8)	2.8325 (8)	2.0029 (8)	2.0029 (8)
Model (2)	3.4692 (4)	3.9998 (8)	2.8283 (4)	2.8347 (4)	2.0090 (4)	1.9999 (4)
		4.0180 (8)				
Model (3)	3.429 (3)	3.9998 (8)	2.8290 (6)	2.793 (9)	1.87 (2)	2.004 (1)
		3.511 (3)	4.0180 (8)		2.877 (9)	2.15 (2)

parameters of −0.87, 0.73 and 0.66 for Ti, O1 and O2 in the correlation matrix (deposited) indicate the strength of the correlation for model (3). That high correlation represents a low radius of curvature on the error surface, illustrating why accurate structure factors are necessary for stable least-squares refinement. It is responsible for the sizeable differences between U_{33} values for the two data sets. Nevertheless the results are more reliable than those obtained in earlier work, where refinements were stable only with some of the structural parameters constrained.

The reliability indices listed in Table 1 provide conflicting evidence on the relative accuracy of the two data sets. The lower merging R indicates that data set (1) is more accurate. For least-squares refinement of the tetragonal structures, however, the refinement indices are almost identical for both data sets. Those for the cubic average are lower for data set (2). Careful comparison of the refinements traced this behaviour to the lower standard deviations for a few low-angle reflections with high weighted residuals in data set (1). Least-squares refinements for that data set are dominated to a greater degree by the limited number of reflections with large residuals. Although data measurements for data set (1) are more precise the Gauss–Markov conditions for least-squares refinement, requiring that the weighted residuals should be normally distributed, are less well satisfied for that data set.

Selected interatomic vector lengths are listed in Table 3. In the centrosymmetric tetragonal structure, ideal octahedral symmetry of the Ti—O system is maintained to within 0.01 Å. In the non-centrosymmetric structure the Ti—O2 and Ba—O1 distances differ by less than 0.01 Å from the ideal values. The two Ba—O2 distances increase and decrease by 0.04 Å, whereas the corresponding Ti—O1 shifts are 0.14 Å. The larger displacements of Ti and O1 in the opposite sense along c presumably reflect the force responsible for the ferroelectric distortion in the structure.

The pattern of the mean-square vibration amplitudes differs qualitatively from those in both the ideal KMF_3 and $SrTiO_3$ perovskites. The change is partly attributable to the larger radius for the Ba atom, for which the mean U_{ij} value is less than those for O and Ti, its largest component (U_{33}) being in the direction of the elongated c axis. The large Ba radius also accounts for the vibration of the O atoms being closer to isotropic than those for F in the KMF_3 series, for which the strongly directed M—F bonds restrict motion mainly in the M—F direction.

The cubic $Pm\bar{3}m$ model is unsatisfactory in having O atoms vibrating maximally along Ti—O bonds – the situation being even more pronounced for O1 in the centrosymmetric tetragonal model. These anomalies are eliminated in the non-centrosymmetric model, in which the vibrations of Ti and O are substantially reduced – albeit with high e.s.d.'s. The vibration amplitudes for O1 in the *ab* plane are higher than those for O2 – which is not unexpected because O2 is more confined by the Ti—O2 bonds in that plane. The U_{11} and U_{22} values for Ti are larger than the corresponding values for both O1 and O2, a result which would appear anomalous if it did not also occur in $SrTiO_3$ (Buttner & Maslen, 1992). The corresponding relationships for U_{33} are less clear because of the large e.s.d.'s for these values in the non-centrosymmetric model. However for the centrosymmetric tetragonal model U_{33} for Ti is also larger than those for both O1 and O2. Because the displacements of Ti, O1 and O2 from the ideal values have comparable magnitudes, it is unlikely that the

centrosymmetric averaging has changed the U_{33} relationship from those in the correct structure. It thus appears that the Ti vibration amplitudes along all the Ti—O bonds are larger than those of the O atoms, as in $SrTiO_3$. However in $BaTiO_3$ the other components of the O-atom vibrations are also low – a contrast with $SrTiO_3$ where larger vibration normal to the Ti—O bonds is permitted by the smaller radius of the Sr cation.

Table 4. *Hirshfeld charges* (e) *for* $BaTiO_3$

Data set (2) follows the data set (1) result for each column entry.

	Model (1)	Model (2)	Model (3)
Ba	0.62 (4)	0.59 (3), 0.94 (3)*	1.27 (3), 1.89 (3)*
	0.31 (4)	0.41 (3), 0.87 (3)*	0.81 (3), 1.70 (3)*
Ti	0.05 (3)	0.02 (4), 0.51 (4)*	−0.14 (3), 0.91 (3)*
	−0.12 (4)	−0.09 (5), 0.51 (5)*	−0.20 (5), 0.96 (5)*
O1	−0.22 (3)	−0.05 (3), −0.41 (3)*	−0.10 (3), −0.68 (3)*
	−0.06 (4)	−0.09 (4), −0.54 (4)*	−0.16 (4), −1.03 (4)*
O2	−0.22 (3)	−0.28 (3), −0.51 (3)*	−0.51 (3), −1.06 (3)*
	−0.06 (4)	−0.12 (4), −0.42 (4)*	−0.22 (4), −0.82 (4)*

* No extinction correction applied.

Atomic charges

Atomic charges, determined by projecting the difference density onto atomic density basis functions following the method of Hirshfeld (1977) are listed in Table 4. The signs of the charges for the Ba and O atoms are consistent with their being electropositive and electronegative respectively. The electron count on the Ti atom is higher (*i.e.* its charge is more negative) than would be expected from its oxidation state and electronegativity. On the other hand the result is consistent with the observations of Buttner, Maslen & Spadaccini (1990), who point out that electrons accumulate preferentially in structural regions which are not tightly packed. Thus Ba, which because of its large radius is tightly packed in this structure, acquires a high positive charge by strong exchange depletion of its electron density.

As previously reported, atomic charges determined for perovskite structures are sensitive to the extinction corrections, to a degree which increases with the atomic number of the atoms in the structure (Maslen & Spadaccini, 1992). Extinction corrections determined for perovskites by least-squares minimization of $\sum w(|F_o| - |F_c|)^2$ tend to reduce the polarity of the structure by increasing the electron count on the heaviest atom, which is usually a cation. The difficulty is compounded because of the sensitivity of the extinction corrections determined by least-squares minimization to the weights of the low-order reflections. Owing to the limitations of the structure-factor model the weighted residuals with accurate structure factors may not satisfy the Gauss–Markov conditions for validity of the least-squares process. Essentially these require that the weighted residuals be normally distributed and comparable to the weighted variances – *i.e.* to unity.

The consequences of inaccurate extinction corrections may be illustrated by evaluating charges determined assuming that there is no extinction in the data. These are included in Table 4. The no-extinction assumption gives charges with magnitudes lower than the formal oxidation states and the signs of these charges are consistent with electronegativities for all atoms. If there is no clear way of distinguishing between the extinction-affected and extinction-free models there is considerable uncertainty in the degree of polarity determined for the structure.

Difference density

The consistency of the difference densities for the two data sets is illustrated by the (110) planes for the centrosymmetric tetragonal model shown in Fig. 1. There are electron deficiencies of −3.2 and −2.8 e Å^{-3} at Ba and of −3.9 and −3.5 e Å^{-3} at the Ti position for data sets (1) and (2) respectively. In the region near the Ti—Ba vector there are peaks approximately 0.35 Å from the Ti nucleus of height 0.9 e Å^{-3} for both experiments. These peaks are unresolved for data set (2) and barely resolved for data set (1). The regions are enclosed by a nearly uniform ring of negative density minimizing 0.6 Å from the Ti nucleus. The $\Delta\rho$ topography near the Ba atom resembles that near Ti, but the ring of depletion 0.58 Å from the Ba nucleus has far more structure, being resolved more clearly for data set (1). There are twin maxima 0.32 Å from the Ba nucleus close to the Ba—Ba vector in the *c* direction. The density at the O1 site is depleted by −0.9 and −0.8 e Å^{-3} for data sets (1) and (2). There is a pronounced depletion of density of depth −1.8 and −1.9 e Å^{-3} at the structural cavity marked X in Fig. 1. Similar depleted regions are reported for other related perovskite structures (Maslen & Spadaccini, 1989; Buttner & Maslen, 1988). There is unusually close correspondence between the Fig. 1 maps and corresponding sections of the 'best' map obtained for $SrTiO_3$ (Buttner, 1990). Near the Ti atom the degree of correspondence between the two maps is remarkable. In the vicinity of the alkaline-earth atom the $BaTiO_3$ map shows more structure, as expected.

A prominent characteristic of these $BaTiO_3$ maps is the depletion extending between the Ba nucleus in the *c* direction containing the strong depletion marked X in Fig. 1. If that broad negative region were predominantly due to the depleting effect of overlap between adjacent Ba atoms it should be weaker than that in the corresponding directions along *a* and *b*, but that is not observed. There is no inconsistency if overlap with O2 atoms above and

below the plane contributes strongly to this depletion. These atoms are closer to the plane of Fig. 1 than the corresponding atoms near the (101) planes. This is illustrated in Fig. 2, where the density is more depleted along the O2—X—O2 vector than along O1—X—O1.

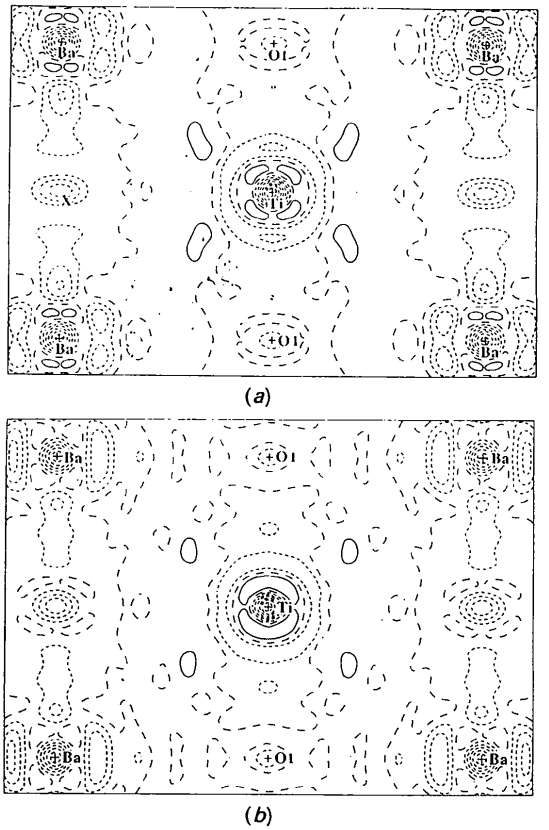

Fig. 1. $\Delta\rho$ centrosymmetric *P4/mmm* refinement of $BaTiO_3$, (110) plane, map borders 7.0 × 5.0 Å. (*a*) Data set (1), (*b*) data set (2). Contour intervals 0.5 e $Å^{-3}$, positive contours solid, zero and negative contours long and short dashes respectively.

$\Delta\rho$ sections for the (100) plane with the non-centrosymmetric model are shown in Fig. 3. The $\Delta\rho$ topography is broadly similar to that for the centrosymmetric model, but there are some marked differences, especially reduced depletion at the O1 and O2 nuclei, splitting of the feature at X into two closely spaced minima, and the displacement of the Ti nuclear position from the centre of its enclosing zone of depleted density.

In the analogous case of the F2 atom in $KCuF_3$ (Buttner, Maslen & Spadaccini, 1990), the topography of $\Delta\rho$ near the F nucleus is such as to produce a force opposing that generated by the promolecule, and thus helping to restore equilibrium. Theoretical calculations based on stationary nuclei indicate the force on the nucleus to be dominated by $\Delta\rho$ components very close to the nucleus. However the potential for small nuclear displacements should be harmonic, to a good approximation, and averaging over harmonic displacements will reduce the dominance of the sharp components in $\Delta\rho$. We therefore consider it worthwhile to examine the effect of longer-range anharmonic components on the density that are observable in diffraction experiments.

In $BaTiO_3$, Ti is asymmetrically positioned along the O1—O1 vector. The promolecule force tends to displace the Ti nucleus in the positive *c* direction. The density in the $\Delta\rho$ (100) section containing Ti shown in Fig. 3 is depleted by -1.1 e $Å^{-3}$ approximately 0.6 Å to the left of the Ti nucleus, and rises to a local maximum of 1.1 e $Å^{-3}$ at 0.3 Å, falling to -3.5 e $Å^{-3}$ at the nuclear position. The density is maximally depleted by -3.8 e $Å^{-3}$ just to the right, rises to 0.6 e $Å^{-3}$ at 0.3 Å, before dropping to -0.8 e $Å^{-3}$ at 0.6 Å. This polarization exerts a force on the Ti nucleus opposing that due to the promolecule.

Ideally there should be similar polarization around the asymmetrically positioned O1 and O2 atoms – a

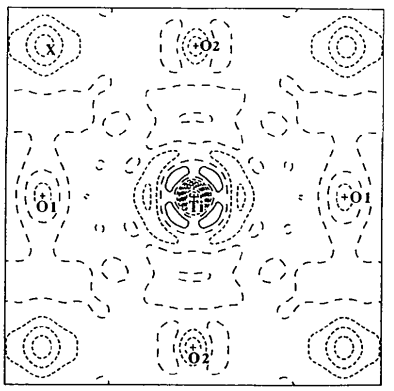

Fig. 2. $\Delta\rho$ for centrosymmetric *P4/mmm* refinement of $BaTiO_3$, (100) plane, map borders 5.0 × 5.0 Å. Contouring as in Fig. 1.

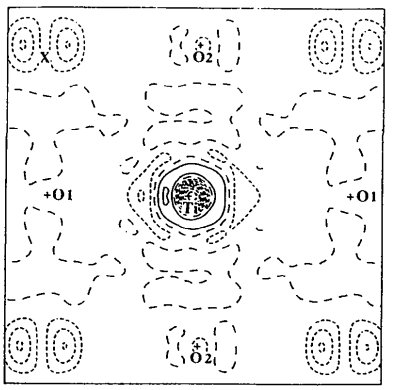

Fig. 3. $\Delta\rho$ for non-centrosymmetric *P4mm* refinement of $BaTiO_3$. (100) plane, map borders 5.0 × 5.0 Å. Contouring as in Fig. 1.

requirement which taxes the data because the atomic number of O is much lower than that of Ba. There is correspondingly high uncertainty in the O-atom positions. To investigate the relevant density requires expanded sections with reduced contour interval as displayed in Fig. 4. For O2 the displacement from the ideal position is in the c direction. This asymmetry of the Ba—O interactions is principally responsible for the promolecule force, giving a resultant in the $-c$ direction. Ba—O bonds being weaker that Ti—O bonds, this force should be correspondingly weak. A broad dipole with excess density to the right of O2 is opposed by a more localized slope to the left. A balance between the forces due to the long- and short-range gradients, combined with the promolecule term, should produce equilibrium.

On the other hand, $\Delta\rho$ for O1, displayed in Fig. 4(*b*), shows only a local gradient to the left at the O1 site – a result inconsistent with stability. To assess the significance of that result the O1 position was displaced by $\sigma(z)$ to the position 0.5, 0.5, 0.0113 and the other least-squares variables were refined. The U_{33} vibration amplitude for O1 increased by about 0.5σ from the refined value in Table 2. In the $\Delta\rho$ map with the adjusted O1 z coordinate the $\Delta\rho$ gradient was strongly reversed. Thus Fig. 4(*b*) is not incompatible with stability at the O positions.

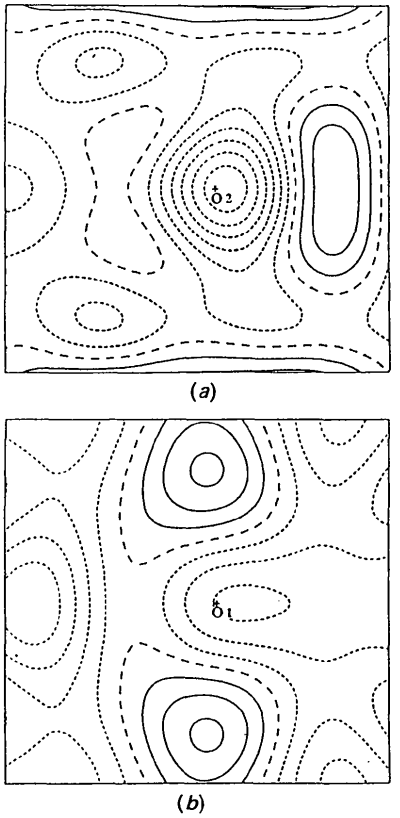

(*a*)

(*b*)

Fig. 4. $\Delta\rho$ for non-centrosymmetric *P4mm* refinement of $BaTiO_3$, (100) plane, positive contour solid, zero and negative contours long and short dashes respectively. Map borders 1.2 × 1.2 Å. Contour intervals 0.1 e $Å^{-3}$. (*a*) O2, (*b*) O1.

The contributions of computer programs by their authors R. Alden, G. Davenport, R. Doherty, W. Dreissig, H. D. Flack, S. R. Hall, J. R. Holden, A. Imerito, R. Merom, R. Olthof-Hazenkamp, M. A. Spackman, N. Spadaccini and J. M. Stewart to the *XTAL*2.6 system (Hall & Stewart, 1989), used extensively in this work, are gratefully acknowledged. This research was supported by the Australian Research Council.

References

ALCOCK, N. W. (1974). *Acta Cryst.* **30**, 332–335.
BUERGER, M. J. (1960). *Crystal Structure Analysis.* New York: John Wiley.
BURBANK, R. D. & EVANS, H. T. JR (1948). *Acta Cryst.* **1**, 330–336.
BUTTNER, R. H. (1990). PhD thesis. Univ. of Western Australia, Australia.
BUTTNER, R. H. & MASLEN, E. N. (1988). *Acta Cryst.* C**44**, 1707–1709.
BUTTNER, R. H. & MASLEN, E. N. (1992). *Acta Cryst.* B**48**, 639–644.
BUTTNER, R. H., MASLEN, E. N. & SPADACCINI, N. (1990). *Acta Cryst.* B**46**, 131–138.
CROMER, D. T. & LIBERMAN, D. (1970). *J. Chem. Phys.* **53**, 1891–1898.
CROMER, D. T. & MANN, J. B. (1968). *Acta Cryst.* A**24**, 321–324.
DANNER, H. R., FRAZER, B. C. & PEPINSKY, R. (1960). *Acta Cryst.* **13**, 1089.
EVANS, H. T. JR (1951). *Acta Cryst.* **4**, 377.
EVANS, H. T. JR (1961). *Acta Cryst.* **14**, 1019–1026.
FRAZER, B. C., DANNER, H. R. & PEPINSKY, R. (1955). *Phys. Rev.* **100**, 745–746.
HALL, S. R. & STEWART, J. M. (1989). Editors. *XTAL*2.6 *User's Manual.* Univs. of Western Australia, Australia, and Maryland, USA.
HARADA, J., PEDERSEN, T. & BARNEA, Z. (1970). *Acta Cryst.* A**26**, 336–344.
HIPPEL, A. R. VON, BRECKENRIDGE, R. G., CHESLEY, F. G. & TISZA, L. (1946). *Ind. Eng. Chem.* **38**, 1089.
HIRSHFELD, F. H. (1977). *Isr. J. Chem.* **16**, 198–201.
LARSON, A. C. (1970). *Crystallographic Computing*, edited by F. R. AHMED. Copenhagen: Munksgaard.
MASLEN, E. N. & SPADACCINI, N. (1989). *Acta Cryst.* B**45**, 45–52.
MASLEN, E. N. & SPADACCINI, N. (1992). *Acta Cryst.* B**48**. Submitted.
MEGAW, H. D. (1945). *Nature* (*London*), **155**, 484–485.
MEGAW, H. D. (1946). *Proc. Phys. Soc.* (*London*), **58**, 133–152.
MEGAW, H. D. (1947). *Proc. R. Soc. London Ser. A*, **149**, 261–283.
RHODES, R. G. (1949). *Acta Cryst.* **2**, 417–419.
SUGI, T., HASEGAWA, S. & OHARA, G. (1968). *Jpn. J. Appl. Phys.* **7**, 358–362.
TANAKA, K. & LEMPFUHL, G. (1972). *Jpn. J. Appl. Phys.* **11**, 1755–1766.
ZACHARIASEN, W. H. (1969). *Acta Cryst.* A**25**, 102–276.